

# Synthesis of multi-walled carbon nanotubes with controlled inner and outer diameters by ethylene decomposition over Ni/MgO and Co/MgO catalysts

N.V. LEMESH\*, P.E. STRIZHAK

L.V. Pisarzhevskii Institute of Physical Chemistry, National Academy of Sciences of Ukraine  
Prosp. Nauki 31, Kiev 03028, Ukraine

In this work, multi-walled carbon nanotubes (MWCNTs) with significantly different mean diameters were produced by catalytic CVD over Ni and Co-based supported catalysts. Our results indicate that Ni nanoparticles in the Ni/MgO catalyst are responsible for controlling the inner diameters of the carbon nanotubes. Contrary, Co nanoparticles in the Co/MgO catalyst control the outer diameters of MWCNTs. The “base-growth” mechanism and smaller diameters of the MWCNTs grown on the Ni/MgO catalyst are associated with a strong metal-support interaction (SMSI) resulting from  $\text{Ni}_x\text{Mg}_{1-x}\text{O}$  mixed oxide formation. The concept of the weak metal-support interaction (WMSI) between Co nanoparticles and MgO for the Co/MgO catalyst confirms the “tip-growth” mechanism of the MWCNTs.

Keywords: carbon nanotubes; nanoparticles; nickel; cobalt; metal-support interaction

## 1. Introduction

Multi-walled carbon nanotubes (MWCNTs) have attracted a widespread interest of researchers owing to their unique structure as well as physical and chemical properties that open a wide range of their potential applications [1–3]. Among numerous techniques of MWCNTs synthesis [4–6], catalytic chemical vapor deposition (CCVD) [7, 8] is the most popular method of their synthesis because it allows one to control their growth and the structure by adjusting reaction conditions (carbon source, reaction temperature, etc.) and catalyst structure (type and size/amount of active phase, chemical nature of the support, etc.). It is a good method for large-scale production of high-quality MWCNTs at relatively low cost [9].

Nickel, iron, and cobalt are well known catalysts for MWCNTs growth by CCVD. These catalysts can absorb and decompose carbon precursors, leading to MWCNTs formation according to the “tip-growth” or “base-growth” model [10]. Zeolites [11],  $\text{Al}_2\text{O}_3$  [12],  $\text{SiO}_2$  [13],

MgO [14, 15], and CaO [16, 17] are the most commonly used supports for the catalysts that can be prepared by impregnation [18] and co-precipitation [19–21] methods.

Numerous works have been devoted to the study of the effect of catalyst and support on the structure of multi-walled carbon nanotubes obtained by CCVD [22]. In particular, synthesis of MWCNTs over a catalyst system with MgO support has often been discussed. MWCNTs over Ni/MgO and Co/MgO catalysts have been obtained using CO as a carbon source [20–23]. It was found that the use of Ni/MgO catalyst results in formation of MWCNTs with the average diameter of 9 nm [23]. MWCNTs with larger diameters (from 10 nm to 50 nm) that strongly depend on Co nanoparticles size were formed at the Co/MgO catalyst [20]. The bimetallic systems, such as Fe–Ni/MgO [24] and Fe–Co/MgO [25, 26], were studied in CCVD synthesis of MWCNTs by acetylene and ethylene decomposition. It was found that MWCNTs diameters are mainly affected by the metal loading and the ratio of metals in these systems. These systems have also been studied with small amounts of Mn and Mo added into

\*E-mail: lemeshnatalia@gmail.com

the catalyst. The addition of Mn in the NiMgO catalyst greatly increased the carbon yield. The Ni nanoparticles size was found to be increased from 15.2 nm for the NiMgO catalyst to 19.9 nm for  $\text{Mn}_{0.2}\text{NiMgO}$  catalyst and further to 29.6 nm for  $\text{Mn}_{0.3}\text{NiMgO}$  [27]. Addition of Mo caused dispersion of active metal precursors which resulted in the formation of MWCNTs of smaller outer diameters [28, 29].

Only a few papers have been devoted to the simultaneous study of the outer and inner diameters of the MWCNTs. Kuras et al. [30] studied the dependence of inner and outer diameters of MWCNTs on different thermal treatments of lanthanum-nickel perovskite catalyst. They found that optimum temperature for the perovskite annealing is 750 °C. Qiang et al. [31] found a possibility to control the inner and outer diameters by changing the Ni:Mo ratio in the Ni/Mo/MgO catalyst. Pan et al. [32] reported the growth of MWCNTs with a larger inner diameter using  $\text{HBO}_3$  as an additional catalyst in CCVD synthesis from a mixture of benzene and ethanol precursors. The structure of all these catalysts was investigated precisely in all these studies. However, in all these studies, there is a lack of data regarding a relationship between the chemical nature of the solid oxide formed during the catalyst preparation, the outer and inner diameters of MWCNTs and the mechanism of their growth.

The aim of this work is to determine the effect of catalyst structure on the MWCNTs morphology and diameters and find the factors responsible for controlling the inner and outer diameters of MWCNTs. For this purpose, all MWCNTs were obtained over the co-precipitated catalysts with different active phases (Ni- and Co-supported MgO) by CCVD ethylene decomposition under the same conditions.

## 2. Experimental

The Ni/MgO and Co/MgO catalysts were prepared by a typical co-precipitation method. To prepare these catalysts, aqueous solution of 3.88 g of  $\text{Ni}(\text{NO}_3)_2 \cdot 6\text{H}_2\text{O}$  or  $\text{Co}(\text{NO}_3)_2 \cdot 6\text{H}_2\text{O}$  were mixed

with 5.12 g of  $\text{Mg}(\text{NO}_3)_2 \cdot 6\text{H}_2\text{O}$  and 4 g of citric acid. The obtained mixture was dissolved in 40 mL of distilled water. The loading ratios of Ni:Mg and Co:Mg (wt.%) were 1:2. The mixture of nitrates and citric acid was evaporated and the resulting solid was calcined at 700 °C in air for 5 hours and, finally, a fluffy sample of the catalyst precursor was obtained.

For reduction, 0.5 g of the catalyst was placed in a quartz boat that then was put in a horizontal quartz reactor with an inner diameter of 25 mm and a length of 900 mm. The sample was then heated upon 700 mL/min flow in a mixture of purified  $\text{H}_2$  (99.99 % purity) with Ar (99.99 %) with volume ratio of 1:2. The heating was carried out from room temperature to 700 °C with a rate of 5 °C/min and keeping the sample at this temperature for 30 min. After this time, hydrogen was turned off, and the system was cooled down to room temperature in an argon atmosphere (100 mL/min). The recovered catalyst was collected for analysis.

For the MWCNTs synthesis, the mixture of hydrogen and argon after catalyst reduction was replaced by a flow of 700 mL/min of a  $\text{C}_2\text{H}_4/\text{H}_2/\text{Ar}$  mixture (1:4:6) and the MWCNTs growth was performed at conditions described above for 30 min. After cooling the system in Ar flow to room temperature, the carbon product was collected for analysis. Obtained carbon nanotubes were used directly for characterizations without purification. The yield of as-synthesized MWCNTs was calculated using the formula:

$$(W_{\text{total}} - W_{\text{cat}})/W_{\text{cat}} \quad (1)$$

where  $W_{\text{cat}}$  is the weight of the catalyst before the reaction and  $W_{\text{total}}$  is the weight of the MWCNTs product after synthesis.

The structures and morphologies of the catalyst after recovery and as-synthesized MWCNTs were characterized using transmission electron microscopy (TEM), scanning electron microscopy (SEM), energy dispersive X-ray spectra and X-ray diffraction (XRD).

Transmission electron microscope (TEM) studies of the MWCNTs and the catalyst were

performed by using TEM-125K (Selmi, Ukraine). Diameter distributions were calculated from the measurement of more than 200 MWCNTs and nanoparticles present in TEM images. The surface morphology and elemental composition of as-synthesized MWCNTs was characterized by the scanning electron microscope FEI NOVA NANOSEM-200 (Holland) equipped with EDX detector. XRD analyses were performed in step scan mode (step:  $0.02^\circ$ , counting time: 10 s) by means of a Bruker D8 Advance diffractometer using  $\text{CuK}\alpha$  radiation source ( $\lambda = 1.5184 \text{ \AA}$ ). Structure of the catalysts was determined by using EVA software [33]. The sizes of catalyst nanoparticles  $D$  were estimated from the Scherrer equation [34]:

$$D = 0.9\lambda / \beta \cos \theta \quad (2)$$

where 0.9 is the Scherrer constant,  $\lambda$  is radiation wavelength,  $\theta$  is angular position of the peak of interest and  $\beta = 2\theta_1 - 2\theta_2$  (in degrees of  $2\theta$ ).

### 3. Results and discussion

Fig. 1 presents TEM images of the as-synthesized MWCNTs over the Ni/MgO and Co/MgO catalysts. From TEM observation, it is noticeable that MWCNTs grown over the Ni/MgO catalyst have a well-visible internal channels without dividing carbon walls, while the structure of MWCNTs grown over Co/MgO belongs to bamboo-like type that is evidenced by the presence of the walls inside the nanotubes (each of which consists of few graphene layers) that divide them into compartments [36].

The inner and outer diameters of the MWCNTs synthesized over the Ni/MgO catalyst vary in the range of approximately 5 nm to 15 nm and 10 nm to 30 nm, respectively, as shown in Fig. 1a. The nanotubes grown over the Co/MgO catalyst have larger inner and outer diameters equal to  $\sim 5$  nm to 25 nm and  $\sim 20$  nm to 40 nm, respectively (Fig. 1b). As observed from these TEM images, the MWCNTs grown over Ni/MgO catalyst have no metal nanoparticles on their tips, whereas the use of the Co/MgO catalyst resulted in the formation

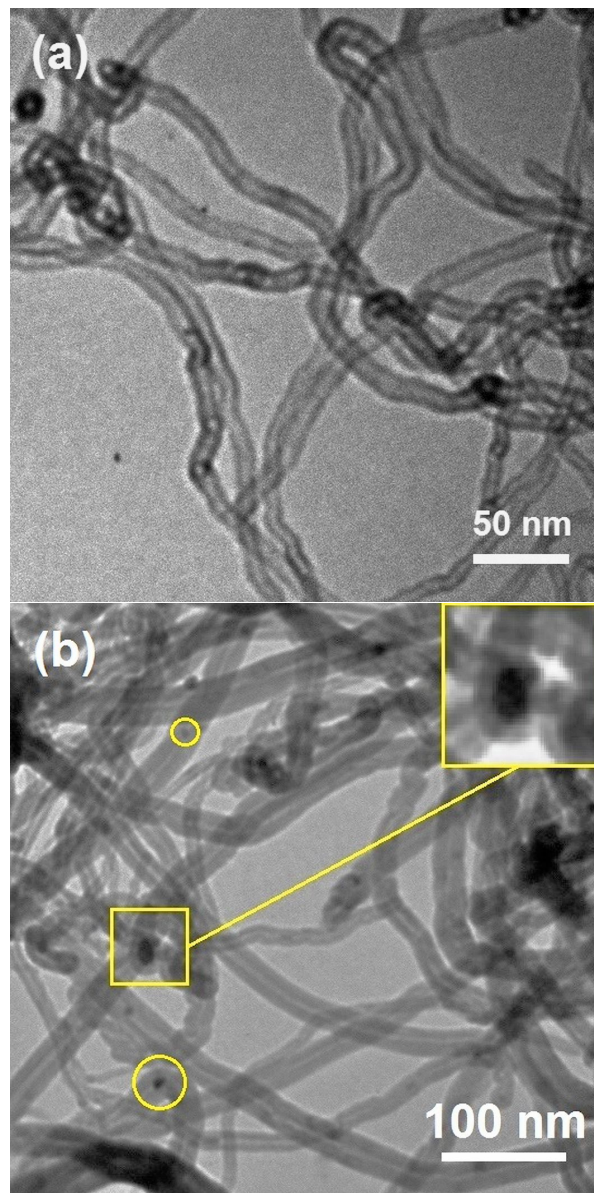


Fig. 1. TEM images of MWCNTs grown over (a) Ni/MgO and (b) Co/MgO catalysts.

of MWCNTs with Co nanoparticles on their tips and inside the internal channels as indicated by the circles in Fig. 1b. In accordance with the data presented in literature, the presence of a nanoparticle on the tip of nanotube indicates the “tip-growth” mechanism [10, 21, 37, 38]. On the other hand, the absence of metal nanoparticles at the ends of nanotubes point to their growth according to the “base-growth” model [10, 38].

Fig. 2a shows the diffraction patterns of the catalyst Ni/MgO before reduction, after reduction and after synthesis on MWCNTs. By using the EVA software [33] the peaks at  $2\theta = 37^\circ$ ,  $43^\circ$  and  $62^\circ$  on the spectra in curve 1 were assigned to the  $\text{Ni}_x\text{Mg}_{1-x}\text{O}$  mixed oxide that was formed during the catalyst preparation. However, these reflexes can overlap with reflexes from magnesium oxide. They have not disappeared after catalyst reduction and MWCNTs synthesis (curve 2). The moderate peak at  $2\theta = 44^\circ$  (Fig. 2a, curve 2 and curve 3) indicates a formation of a small amount of metallic nickel during reduction of the catalyst in the  $\text{H}_2$  flow [33]. It is clear that no remarkable peaks of carbon appeared in the XRD spectra of the MWCNTs, which confirms the relatively small MWCNTs yield, equal to 0.52 g-MWCNTs/g-catalyst. The presence of the  $\text{Ni}_x\text{Mg}_{1-x}\text{O}$  in all samples and very small reflexes corresponding to metallic nickel indicates a very poor reduction of the  $\text{Ni}_x\text{Mg}_{1-x}\text{O}$  due to the excellent mutual solubility between NiO and MgO [14].

The peaks present in Fig. 2b at  $43^\circ$  and  $62.2^\circ$  correspond to the mixed oxide  $\text{Co}_x\text{Mg}_{1-x}\text{O}$  [33] or a mixture of this oxide with MgO. In the XRD pattern of reduced Co/MgO (curve 2), the peaks for CoO ( $2\theta = 36^\circ$  and  $43^\circ$ ), Co ( $2\theta = 44^\circ$ ), and MgO ( $2\theta = 42.6^\circ$  and  $62^\circ$ ) are clearly visible [33], which indicates decomposition of the  $\text{Co}_x\text{Mg}_{1-x}\text{O}$  to Co and MgO. The CoO formation most likely occurs as a result of oxidation of metallic cobalt in air during catalyst storage. The peak at  $2\theta = 26^\circ$  for C (MWCNTs) is present in the spectra of as-synthesized MWCNTs (curve 3) [33]. The presence of this peak is in accord with the higher yield of the carbon nanotubes: 2.2 g-MWCNTs/g-catalyst. This peak is not sharp which confirms defective structure of the MWCNTs [14, 34].

The difference in the diameters and morphology of the MWCNTs in the two samples has been confirmed by SEM images presented in Fig. 3. As seen in Fig. 3a, the nanotubes grown over Ni/MgO catalyst have a smooth surface. They are more uniform in diameters than MWCNTs

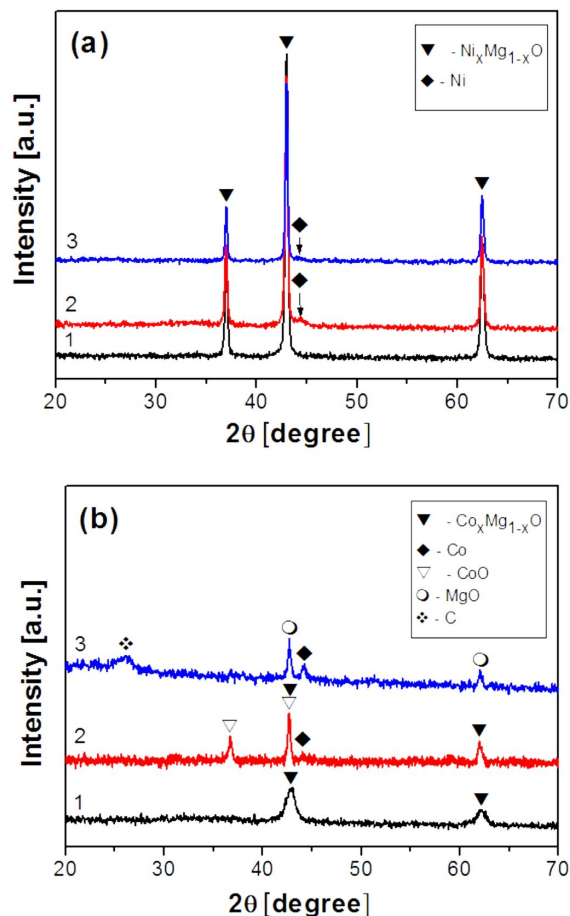


Fig. 2. XRD patterns of (a): 1. Ni/MgO catalyst before reduction; 2. Ni/MgO catalyst after reduction; 3. As-synthesized MWCNTs obtained over Ni/MgO catalyst and (b): 1. Co/MgO catalyst before reduction; 2. Co/MgO catalyst after reduction; 3. As-synthesized MWCNTs obtained over Co/MgO catalyst.

grown over Co/MgO (Fig. 3b). Some impurities of the catalyst can be distinguished in the SEM image of MWCNTs obtained over Ni/MgO catalyst while MWCNTs grown on the Co/MgO catalyst have a higher purity. This is explained by the much higher yield of MWCNTs synthesized on the Co/MgO catalyst.

The energy-dispersive X-ray (EDX) spectroscopy of the MWCNTs confirms the presence of C, O, Mg, Ni and Co (Fig. 4) in the MWCNTs samples. The percentages by weight of the elements for each sample are

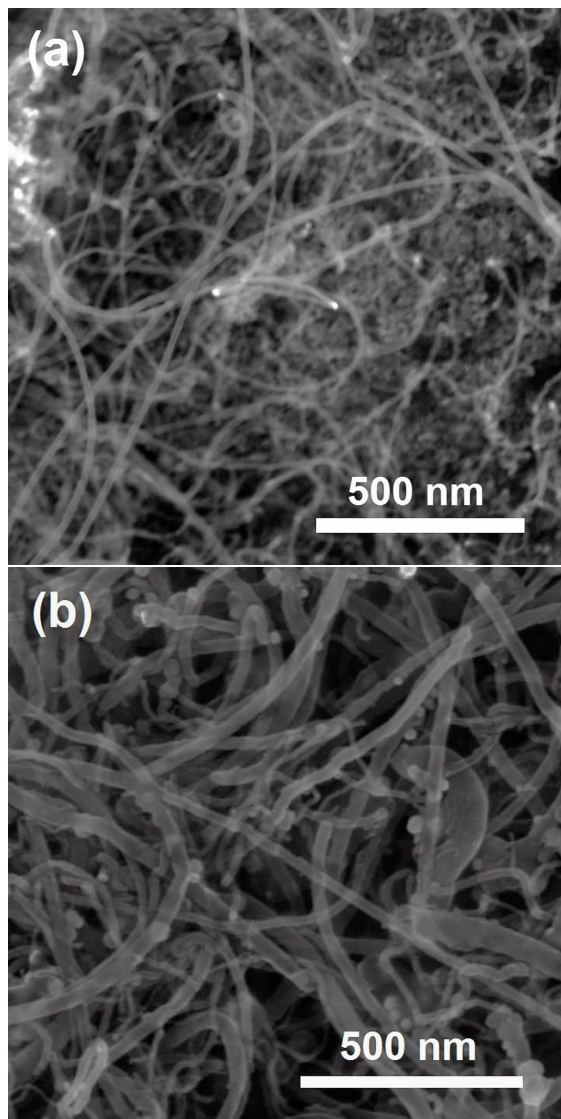


Fig. 3. SEM images of MWCNTs grown over (a) Ni/MgO, and (b) Co/MgO catalysts.

given in the upper right corner of the EDX spectrum. It can be seen that the percentage of carbon in the MWCNTs obtained over Co/MgO (Fig. 4b) is significantly higher than the content of C in the MWCNTs grown over Ni/MgO (Fig. 4a). This is owing to a higher yield of MWCNTs obtained using the Co/MgO catalyst.

Fig. 5a displays a TEM image of the Ni/MgO catalyst after H<sub>2</sub> reduction. This microphotograph shows clusters that consist of aggregated crystallites. The small dark nanoparticles (pointed

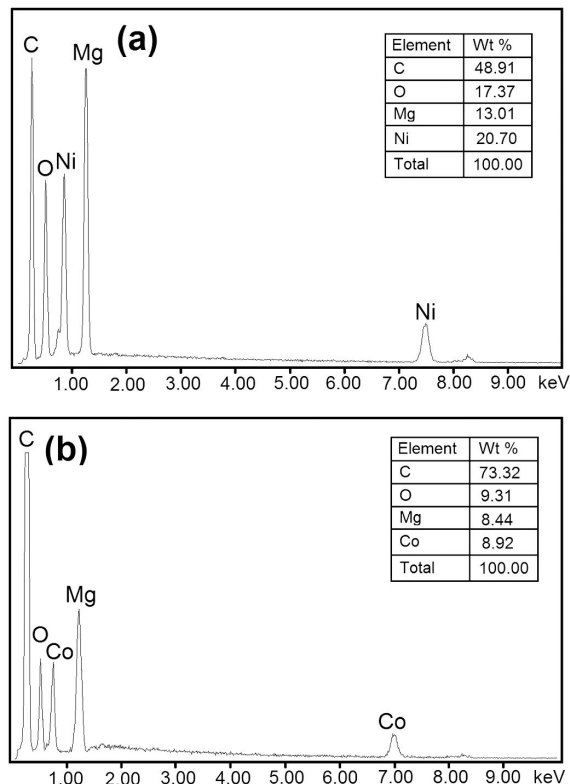


Fig. 4. Energy dispersive X-ray spectra of MWCNTs grown over (a) Ni/MgO, and (b) Co/MgO catalysts.

by circles) can be distinguished on the surface of these crystallites. The crystallites, according to the XRD spectra (Fig. 2a), were assigned to Ni<sub>x</sub>Mg<sub>1-x</sub>O and the dark nanoparticles were attributed to metallic Ni [15].

The faceted structure of the reduced Co/MgO catalyst is presented in the TEM image (Fig. 5b). The crystallinity of the Co/MgO catalyst nanoparticles is more complex and therefore it is difficult for us to distinguish the crystal phases of Co, CoO, and MgO detected by XRD for the reduced catalyst (Fig. 2b, curve 1).

Table 1 summarizes the mean values of MWCNTs diameters and catalyst nanoparticles sizes calculated from TEM images and estimated from XRD spectra by the Scherrer equation. From the data presented in Table 1, it is concluded that the value of the size of Ni crystallite estimated

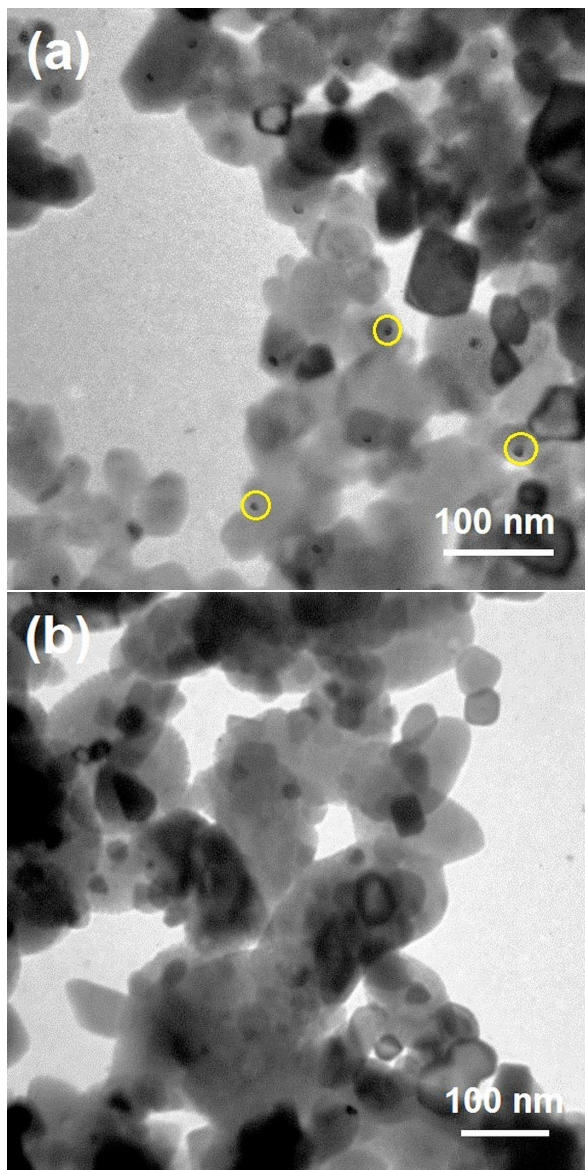


Fig. 5. TEM images of (a) Ni/MgO; and (b) Co/MgO catalysts after reduction.

by the Scherrer equation [35] that equals to 7 nm, almost coincides with the value of the mean inner diameter of the MWCNTs grown over the Ni/MgO catalyst (6 nm). The value of the Co crystallite size has been found between the mean values of inner and outer diameters of the MWCNTs synthesized over the Co/MgO catalyst. The mean size of metal nanoparticles of the Ni/MgO and Co/MgO catalysts calculated from TEM images decreased during the reduction probably as a result of formation of smaller active phase nanoparticles.

Fig. 6a shows the Gaussian distribution of the MWCNTs diameters and Ni/MgO catalyst nanoparticles sizes. From the data presented, it can be inferred that the size distribution of the reduced Ni/MgO catalyst (curve 3) is bimodal. The second mode of this curve was attributed to the  $\text{Ni}_x\text{Mg}_{1-x}\text{O}$  species distribution. The first mode that varies in the range of 5 nm to 20 nm, was assigned to the size distribution of nickel nanoparticles formed during recovery. The maximum of the first mode of this distribution is 9 nm. These values are close to the  $D_{\text{Ni}}$ , estimated by the Scherrer equation that equals to 7 nm (Table 1). The first mode of the catalyst nanoparticles distribution overlaps with the distribution of the inner diameters of the MWCNTs (curve 1). Therefore, the size of nickel nanoparticles in the Ni/MgO catalyst determines the inner diameter of MWCNTs. Analysis of the TEM image in Fig. 1a allows one to conclude that MWCNTs have grown according to the “base-growth” mechanism because there are no nickel nanoparticles found at the tubes tips [10, 37]. The single-walled CNTs or nanotubes with several layers have formed by this mechanism on the small metal nanoparticles, with diameters of 5 nm to 10 nm, since the “base-growth” allows easily realizing surface diffusion of carbon [10]. In consequence of the diffusion of carbon atoms over the surface of a nanoparticle, the first graphene layer in a shape of a cap covering the metal nanoparticle has formed. The following layer has grown under the previous one and replaced it. As a result, the first layer lifted away from the particle. Thus, the size of the metal nanoparticle remains the same, and its edge touches the first sheet of graphene, the one which was formed last. This layer determines the inner diameter of the MWCNT. Therefore, in case of the “base-growth” mechanism, the metal nanoparticle size determines the inner diameter of the nanotubes. The relation between the growth mechanism and the metal-support interaction (MSI) has been reported in the literature [10, 21, 38]. When the “base growth” mechanism takes place, the strong metal-support interaction (SMSI) occurs and the SMSI interaction of the metal with a support is determined by chemical bonds of metal atoms and atoms of support in the mixed

Table 1. The size of active metal nanoparticles and MWCNTs diameters obtained from the XRD and TEM of the Ni/MgO and Co/MgO catalysts.

Catalyst	Ni/MgO	Co/MgO
Mean size of the catalyst before reduction (TEM) $\pm$ standard deviation, [nm] (total)	47 $\pm$ 13	43 $\pm$ 10
Mean size of the catalyst after reduction (TEM) $\pm$ standard deviation, [nm] (total)	36 $\pm$ 23	39 $\pm$ 1 4
Mean size of the nanoparticles on the tips or inside MWCNTs (TEM) $\pm$ standard deviation in [nm]	–	31 $\pm$ 9
Mean external diameters of MWCNTs (TEM) $\pm$ standard deviation in [nm]	14 $\pm$ 3	30 $\pm$ 8
Mean internal diameters of MWCNTs (TEM) $\pm$ standard deviation in [nm]	6 $\pm$ 1	13 $\pm$ 3
D <sub>Me</sub> after reduction (XRD) in [nm]	7	18
D <sub>Me</sub> after MWCNTs synthesis, (XRD) in [nm]	–	18

oxide [10, 21]. This relationship should contribute to a strong retention of nickel nanoparticles on the support, leading to the “base-growth” mechanism.

Fig. 6b displays Gaussian curves of diameter distributions of MWCNTs grown over the Co/MgO catalyst and the size distribution of Co-nanoparticles present on the MWCNTs tips. The size distribution of cobalt nanoparticles on the tips (curve 3) coincides with the outer MWCNTs diameters distribution (curve 2), whereas it does not overlap with curve 1 for the distribution of the inner diameters. It confirms that the Co nanoparticle sizes determine the outer MWCNTs diameters. As already noted, the presence of Co nanoparticles on the MWCNTs tips (Fig. 1b) serves as a proof of the “tip-growth” mechanism which takes place in case of weak metal-support interaction [20].

It allows suggesting that the metal nanoparticles size determines the outer diameters of MWCNTs. If the “tip-growth” is realized, the surface carbon layer envelopes the nanoparticles at the edges and the inner carbon layer is located inside them. Therefore, in case of the “tip-growth” mechanism, the cobalt nanoparticles size determines the outer diameter of the nanotubes. According to the XRD results (Fig. 2b), the mixed oxide  $\text{Co}_x\text{Mg}_{1-x}\text{O}$  decomposes during the catalyst reduction to Co and MgO and the interaction between them is determined only by the weak van der Waals forces. The WMSI results in the “tip-growth” of MWCNTs on the Co/MgO catalyst.

In some cases, Co nanoparticles are found inside the MWCNTs (Fig. 1b). The proposed growth

mechanism for the nanotubes with nanoparticles in the middle part has been described in the literature [39]. At the temperature of synthesis (700 °C), Co particles and different kinds of hydrocarbons exist in the reaction zone of reactor. When the tube has an open end and the gas phase supplies carbon, the metal particles incorporate into these open tube ends. Simultaneously, carbon dissolves in the particles, diffuses through them, and precipitates again as graphene layers, increasing the tube length. When a liquid-like cobalt particle falls on the tip of the tube, it can be deformed due to squeezing of the tip. The deformed particle is a start point for a new nanotube growth. This model explains the growth of partially and completely filled tubes and very long tubes.

## 4. Conclusions

In this paper, we have examined the effect of the size of Co and Ni nanoparticles on the inner and outer diameters of MWCNTs prepared by the CCVD process over Ni/MgO and Co/MgO co-precipitated catalysts using ethylene as a carbon source. The size of the catalyst nanoparticles strongly depends on the compounds formed during the catalyst preparation. The chemical nature of these compounds determines the strength of the metal-support interaction. The MSI has a great impact on the MWCNTs growth mechanism and their diameters.

In case of Ni/MgO catalyst, the synthesized MWCNTs exhibit relatively small outer (14 nm)

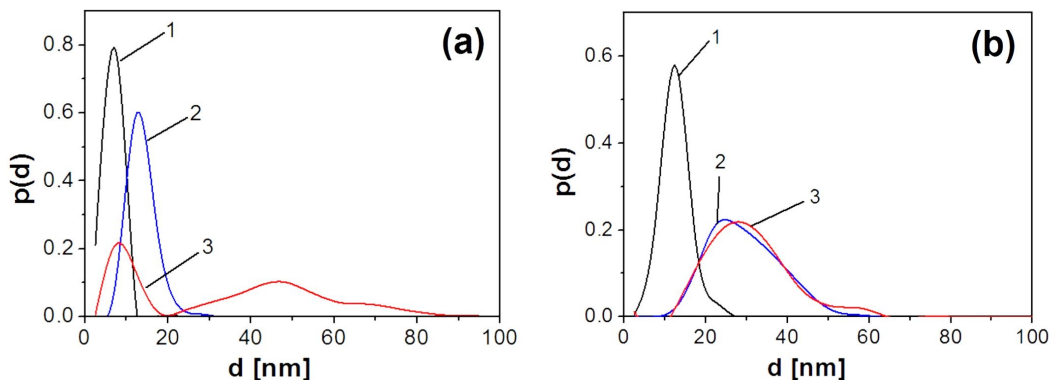


Fig. 6. Gaussian curves of diameters distributions of (a): 1. Inner diameters of MWCNTs grown over Ni/MgO catalyst; 2. Outer diameters of MWCNTs grown over Ni/MgO catalyst; 3. Nanoparticles of Ni/MgO catalyst after reduction; and (b): 1. Inner diameters of MWCNTs grown over Co/MgO catalyst; 2. Outer diameters of MWCNTs grown over Co/MgO catalyst; 3. Cobalt nanoparticles on the tips of MWCNTs.

and inner mean diameters (6 nm). Experimental results suggest that using Ni/MgO as a catalyst results in the formation of  $Ni_xMg_{1-x}O$  mixed oxide that only partially decomposes in the regenerative atmosphere with formation of Ni nanoparticles of relatively small sizes. The MWCNTs were grown on these nanoparticles by the “base-growth” mechanism due to strong metal-support interaction (SMSI). As a result, the size of Ni-nanoparticles controlled the inner diameters of MWCNTs, whereas the outer diameters were independent of the metal nanoparticles size.

Contrary to the Ni/MgO catalyst, the Co/MgO catalyst promotes carbon nanotube growth with larger outer (30 nm) and inner (13 nm) diameters. The Co/MgO catalyst also shows the  $Co_xMg_{1-x}O$  mixed oxide formation, while the catalyst preparation. During the Co/MgO catalyst recovery, the mixed oxide is completely decomposed to Co and MgO. It evidences the weak metal-support interaction (WMSI) between Co and support. The Co nanoparticles size determines the outer MWCNTs diameters and does not control their inner diameters. The mechanism of the MWCNTs growth at this catalyst is attributed to the “tip-growth”.

Our results show an opportunity to control the MWCNTs diameters, morphology and their growth mechanism by changing the metal-support interaction. These finding opens a new way to control both the inner and outer diameters of MWCNTs,

by changing the metal-support interaction and formation of the surface mixed oxides for the catalysts over which MWCNTs may be produced with an appreciable yield for their industrial applications.

#### Acknowledgements

The work is supported by the target integrated program of fundamental research of the National Academy of Sciences of Ukraine: “Fundamental problems of creation of the new compounds and materials of the chemical industry.”

#### References

- [1] LIU L.Q., MA W.J., ZHANG Z., *Small*, 7 (2011), 1504.
- [2] CHATTOPADHYAY S., SINGH K.K., *JMMCE*, 11 (2012), 961.
- [3] ARENA A., DONATO N., SAITTA G., GALVAGNO S., MILONE C., PISTONE A., *Microelectron. J.*, 39 (2008), 1659.
- [4] BERKMANS A.J., RAMAKRISHNAN S., JAIN G., HARIDOSS P., *Carbon*, 55 (2013), 185.
- [5] PASHA A., POURSALEHI R., VESAGHI M.A., SHAFIEKHANI A., *Physica B*, 405 (2010), 3468.
- [6] ZIMMER K., BÖHME R., RAUSCHENBACH B., *Physica E*, 40 (2008), 2223.
- [7] SHOKRY S.A., MORSI A.K., SABAA M.S., MOHAMED R.R., SOROGY H.E., *Egypt. J. Petrol.*, 23 (2014), 183.
- [8] ABDULLAYEVA S.H., MUSAYEVA N.N., JABBAROV R.B., MATSUDA T., *WJCMF*, 4 (2014), 93.
- [9] RAFIQUE M.M.A., IQBAL J., *JEAS*, 1 (2011), 29.
- [10] BAKER R.T.K., *Carbon*, 27 (1989), 315.
- [11] WANG Z., NAVARRETE J., *GSC*, 2 (2012), 91.
- [12] KUDUS M.H.A., AKIL H.M.D., MOHAMAD H., LOON L.E., *J. Alloy. Compd.*, 509 (2011), 2784.
- [13] MESSINA G., MODAFFERI V., SANTANGELO S., TRIPODI P., DONATO M.G., LANZA M., GALVAGNO S., MILONE C., PIPEROPOULOS E., PISTONE A., *Diam. Relat. Mater.*, 17 (2008), 1482.

- [14] AWADALLAH A.E., ABOUL-ENEIN A.A., EL-DESOUKI D.S., ABOUL-GHEIT A.K., *Appl. Surf. Sci.*, 296 (2014), 100.
- [15] YAN X., LIU C.-J., *Diam. Relat. Mater.*, 31 (2013), 50.
- [16] PIPEROPOULOS E., SANTANGELO S., LANZA M., FAGGIO G., MESSINA G., GALVAGNO S., PISTONE A., MILONE C., *Diam. Relat. Mater.*, 20 (2011), 532.
- [17] BIRIS A.R., LUPU D., DERVISHI E., LI Z., XU Y., TRIGWELL S., MISAN I., BIRIS A.S., *Phys. Lett. A*, 372 (2008), 6416.
- [18] BAHGAT M., FARGHALI A.A., ROUBY W.M.A., KHEDR M.H., *J. Anal. Appl. Pyrol.*, 92 (2011), 307.
- [19] NARKIEWICZ U., PODSIADLY M., JEDRZEJEWSKI R., PELECH I., *Appl. Catal. A- Gen.*, 384 (2010), 27.
- [20] PINHEIRO J.P., SCHOULER M.C., GADELLE P., *Carbon*, 41 (2003), 2949.
- [21] RATKOVIC S., VUJICIC D.J., KISS E., BOSKOVIC G., GESZTI O., *Mater. Chem. Phys.*, 129 (2011), 398.
- [22] SHAH K.A., TALI B.A., *Mat. Sci. Semicon. Proc.*, 4 (2016), 67.
- [23] ALLAEDINI G., TASIRIN S.M., AMINAYI P., *J. Alloy. Compd.*, 647 (2015), 809.
- [24] TSOUFIS T., XIDAS P., JANKOVIC L., GOURNIS D., SARANTI A., BAKAS T., KARAKASSIDES M.A., *Diam. Relat. Mater.*, 16 (2007), 155.
- [25] KATHYAYINI H., NAGARAJUA N., FONSECAB A., NAGY J.B., *J. Mol. Catal. A- Chem.*, 223 (2004), 129.
- [26] MACCALLINI E., TSOUFIS T., POLICICCHIO A., LA ROSA S., CARUSO T., CHIARELLO G., COLAVITA E., FORMOSO V., GOURNIS D., AGOSTINO R.G., *Carbon*, 48 (2010), 3434.
- [27] RAN M., CHU W., LIU Y., LIU D., ZHANG C., ZHENG J., *J. Energy Chem.*, 23 (2014), 781.
- [28] YEOH W.-M., LEE K.-Y., CHAI S.-P., LEE K.-T., MOHAMED A.R., *J. Alloy. Compd.*, 493 (2010), 539.
- [29] CHEN R., XIE Y., ZHOU Y., WANG J., WANG H., *J. Energy Chem.*, 23 (2014), 244.
- [30] KURAS M., PETIT P., PETIT C., *Carbon*, 49 (2011), 1453.
- [31] QIANG Z., YI L., LING H., WEI-ZHONG Q., GUO-HUA L., FEI W., *New Carbon Mater.*, 23 (2008), 319.
- [32] PAN Y., LIU Y., CHI W., SHEN Z., *Mater. Lett.*, 65 (2011), 3362.
- [33] ICDD PDF-2 Version 2.0602 (2006).
- [34] CHEN Y., RIU D.-H., LIM Y.-S., *Met. Mater. Int.*, 14 (2008), 385.
- [35] FERET F.R., *Analyst*, 123 (1998), 595.
- [36] LI X., LIU Y., FU L., CAO L., WEI D., WANG Y., *Carbon*, 46 (2008), 255.
- [37] CASSELL A.M., RAYMAKERS J.A., KONG J., DAI H., *J. Phys. Chem. B*, 103 (1999), 6484.
- [38] GOHIER A., EWELS C.P., MINEA T.M., DJOUADI M.A., *Carbon*, 46 (2008), 1331.
- [39] LEONHARDT A., HAMPEL S., MÜLLER C., MÖNCH I., KOSEVA R., RITSCHEL M., ELEFANT D., BIEDERMANN K., BÜCHNER B., *Chem. Vap. Depos.*, 12 (2006) 380.

Received 2018-05-25  
Accepted 2018-09-13